LITHOS 438-439 (2023) 107014

Contents lists available at ScienceDirect

LITHOS

journal homepage: www.elsevier.com/locate/lithos

Syn-mineralization hydrous fluid activity in giant Jinchuan magmatic Ni-Cu sulfide deposit in North China Craton

Qing-Han Yuan [a,b,*], Ben-Xun Su [a,b,*], Meng-Meng Cui [a,b], Patrick Asamoah Sakyi [c], Jie-Jun Jing [d]

[a] Key Laboratory of Mineral Resources, Institute of Geology and Geophysics, Chinese Academy of Sciences, Beijing 100029, China
[b] University of Chinese Academy of Sciences, Beijing 100049, China
[c] Department of Earth Sciencev, University of Ghana, P.O. Box LG 58, Legon-, Accra, Ghana
[d] Faculty of Science, Vrije Universiteit Amsterdam, De Boelelaan 1085, 1081, HV, Amsterdam, the Netherlands

ARTICLE INFO

Keywords:
Ni-Cu sulfide deposit
Selective alteration
Elemental exchange
Fluid activity
Hydrous mineral

ABSTRACT

Giant magmatic Ni-Cu sulfide deposits in the world are hosted mainly in pristine gabbro-dolerite sills (e.g., the first largest in the Noril'sk region) and norite bodies (e.g., the second largest in Sudbury, Duluth, and Voisey's Bay), implying the petrogenic relationship between the giant deposits and anhydrous parental magmas. In contrast, the third largest Jinchuan deposit is hosted in dunite- and lherzolite-dominated peridotite bodies and characterized by the presence of hydrous minerals (e.g., hornblende and phlogopite) and intensive serpentinization of olivine. The role of water in the formation of the magmatic Ni-Cu sulfide deposit remains unclear. To reveal the potential linkage between sulfide mineralization and 'water' (i.e., hydrous minerals), a detailed petrographic investigation of the Jinchuan deposit and the associated mineral chemistry analyses have been conducted in this study. The distribution of serpentinization of olivine in the Jinchuan deposit is unevenly, being more pervasive in the sulfide-bearing rocks compared to sulfide-free rocks. The degree of serpentinization decreases systematically in general sequence outwardly from the core net-textured dunite to the outer disseminated lherzolite at orebody-scale. In the sulfide-bearing rocks, the serpentinization is more intensively observed in the sulfide-rich portions compared to the sulfide-poor portions at thin section-scale. We consider sulfide content-dependent serpentinization as 'selective alteration', which is distinct from post-magmatic modifications and should have occurred coevally with sulfide liquid emplacement and sulfide crystallization. The selective alteration with dependence on sulfide contents is caused by hydrous fluids released from sulfide crystallization, because the crystallized sulfides cannot structurally accommodate hydrous components which previous latching onto the sulfide liquid. The olivine grains in sulfide-bearing rocks are reversely zoned with respect to Ni (Ni-poor cores, Ni-rich rims) and Co (Co-rich cores, Co-poor rims) which can be interpreted by stages of sulfide liquid-olivine Ni-Co exchange and Fe-Ni exchange. Comparison of intra-grain elemental distributions of olivine grains shows that hydrous fluid activity enhanced elemental exchange between olivine and sulfide liquid. Interestingly, the presence of hydrous minerals, protects olivine from selective alteration, suggesting that the hydrous minerals were formed during *syn*-mineralization fluid activity. These features are linkage between the inferred fluids compounded with sulfide droplets in previous experiments and their transfer and fate in natural magmatic sulfide deposits. The selective alteration proposed here, formed during the *syn*-mineralization stage and indicate that the fluid activity is instrumental in the formation of magmatic sulfide ores. The selective alteration may be a common characteristic in ultramafic rock-hosted magmatic sulfide deposits and a pathfinder for mineral exploration.

1. Introduction

Magmatic sulfide deposits form following segregation and concentration of sulfide droplets from mafic-ultramafic magmas and partitioning of ore-forming elements into immiscible sulfide liquid (Naldrett et al., 2011). Most world-scale magmatic Ni-Cu sulfide

* Corresponding authors.
E-mail addresses: yuanqinghan@mail.iggcas.ac.cn (Q.-H. Yuan), subenxun@mail.iggcas.ac.cn (B.-X. Su).

https://doi.org/10.1016/j.lithos.2022.107014
Received 28 September 2022; Received in revised form 28 December 2022; Accepted 28 December 2022
Available online 31 December 2022

deposits in the world are genetically related to pristine mafic rocks. For example, the Noril'sk-Talnakh Ni-Cu sulfide deposit, being the largest in the world, is hosted in gabbros and dolerites (Duzhikov et al., 1992), whilst the others are mainly hosted in norites and quartz diorites (e.g., Sudbury deposit, Lightfoot and Doherty, 2001), troctolitic and gabbroic rocks (e.g., Duluth deposit, Ripley et al., 2007) and troctolites (e.g., Voisey's Bay deposit, Lightfoot and Naldrett, 1999). In contrast, Jinchuan deposit, as the third largest magmatic Ni-Cu sulfide deposit is distinctively hosted in ultramafic dunite- and lherzolite-dominated peridotite body (e.g., Chai and Naldrett, 1992; Tang and Li, 1995). The different lithologies of the host rocks between the Jinchuan deposit and other deposits imply the differences in the nature and evolution of their parental magmas.

Volatiles (e.g., water, halogens) are essential components in most mafic and ultramafic magmas (Lowenstern, 2001; Métrich and Wallace, 2008; Wallace et al., 2015). The presence of water in basaltic melts can alter their liquid lines of descent (Gaetani et al., 1993). The addition of water in anhydrous basaltic melts would change their cumulates evolution path from dunite-troctolite-gabbro to dunite-wehrlite-gabbro (Gaetani et al., 1993; Niu, 2005). The host rocks of most sulfide deposits except Jinchuan are consistent well with the evolution path of cumulates (dunite-troctolite-gabbro) of anhydrous magmatic systems, indicating the parental magma of Jinchuan sulfide is likely hydrous. However, the contribution of hydrous components and to what extent it contributes to the formation of giant magmatic sulfide deposit remains enigmatic.

In addition to altering the liquid and cumulate compositions, volatiles can also modify the density and viscosity of magmas significantly (Dingwell et al., 1996; Giordano et al., 2008; Hui and Zhang, 2007; Lesher and Spera, 2015). On basis of experimental studies, Mungall et al. (2015) hypothesized that spontaneous attachment of sulfide droplets to vapor bubbles because of surface tensions would form low-density compound drops, which are feasible for the upward migration of sulfide liquid. This hypothesis has been verified by the occurrence of globular compound sulfide drops in the Noril'sk deposit (Barnes et al., 2019; Le Vaillant et al., 2017; Schoneveld et al., 2020). Nevertheless, the fate of volatiles that make up of compound drops after metallogenic processes has not been addressed well in the literature. The crystallization of hydrous minerals and water-related alteration cannot be commonly observed in most sulfide deposits which hinders the investigation on the potential *syn*- or post-mineralization hydrous fluid activities. The Jinchuan intrusion composed of typical cumulates from hydrous basaltic magmatic system have abundant hydrous minerals (e.g., phlogopite and hornblende) and intensive serpentinization. To reveal the effects of hydrous fluids in Ni-Cu sulfide mineralization and the fate of fluids afterward, we present detailed petrographic and mineralogical characteristics of hydrothermal alteration of Orebody 1 in the Jinchuan deposit. In this study, the origin, role and fate of hydrous fluids in the formation of magmatic sulfide deposits have been constrained by establishing the genetic link among the presence of hydrous minerals, olivine serpentinization and sulfide mineralization.

2. Geology of the Jinchuan Ni-Cu sulfide deposit

The Jinchuan magmatic Ni-Cu sulfide deposit is located at the eastern part of the Longshoushan Terrane in the North China Craton (Fig. 1a). The Longshoushan Terrane consists mainly of Paleoproterozoic and Mesoproterozoic metamorphic units and is unconformably overlain by Neoproterozoic and Paleozoic conglomerates, sandstones, and limestones (Fig. 1b; Chai and Naldrett, 1992; Tang and Li, 1995; Song et al., 2006). The mafic-ultramafic magmatism in the Longshoushan Terrane is dominantly Neoproterozoic, represented by the Jinchuan ultramafic intrusion (e.g., Li et al., 2005; Zhang et al., 2010).

The Jinchuan intrusion (827 Ma, Li et al., 2004b; 812 Ma, Li et al., 2005; 832 Ma, Zhang et al., 2010) intruded Paleoproterozoic migmatites, gneisses and marbles of the Longshoushan Group. The intrusion is about 6500 m long, 20 to 500 m wide, and generally strikes NW-SE (Fig. 1c). The vertical downward extension of the intrusion is more than 1100 m in its central part (Fig. 1d). The intrusion is composed almost entirely of peridotites, including dunite, lherzolite, and olivine wehrlite, with minor pyroxenite and troctolite (Tang and Li, 1995). It is divided by a series of NE-SW-trending, subvertical strike-slip faults F_8, F_{16-1}, and F_{23} into Segments III, I, II and IV from west to east (Fig. 1c, d). To the west of fault F_{16-1}, Segments III and I consist mainly of fine-grained dunite and lherzolite with minor pyroxenite in the sulfide-free upper unit and coarse-grained lherzolite and dunite in the sulfide-bearing lower unit (Chen et al., 2009, 2013; Song et al., 2012). Segment I contains Orebody 24 (Fig. 1d) that occurs above the basal pyroxenite and may be in contact with the footwall of the country rocks (Chen et al., 2013). On the opposite site of fault F_{16-1}, Segments II and IV comprise mainly of medium- to coarse-grained lherzolite and dunite (Song et al., 2009). Segment II hosts the largest sulfide Orebody 1 in the western part, while the second largest sulfide Orebody 2 is hosted in the eastern part (Fig. 1d). The bulk of the economic resource in the Jinchuan deposit is made up of net-textured ores with typical sulfide contents of about 15–40 vol%, extensive low-grade disseminated ore haloes with typical sulfide contents of about 5–15 vol%, and extremely high-grade disseminated ores with typical sulfide contents of about 70–90 vol%. The net-textured ores usually occur in the interior parts of the intrusion, whereas disseminated ores typically occur in the exterior parts of the intrusion (Fig. 1d). Sulfide minerals are mainly pyrrhotite, pentlandite and chalcopyrite.

3. Samples descriptions and analytical methods

3.1. Sample descriptions

Seventy-eight samples investigated in this study were collected from the interior of Orebody 1 in the Segment II of the Jinchuan intrusion at three levels in the underground tunnels. Samples JC01, JC03, JC05 and JC07 were sampled at elevations of 1018 m (Fig. 2a), 934 m (Fig. 2b), 814 m (Fig. 2c) and dump, respectively. Sample JC04 is from the enclosing intrusive host abutting the hanging wall of Orebody 1 at 934 m (Fig. 2b). From the above-mentioned samples, the following sub-samples, JC01–16, JC03–2, JC03–3, JC03–5, JC03–10, JC03–18, and JC03–19 were recovered from the interior fault zones (Fig. 2a-b); whereas sub-samples JC01–11, JC01–12, JC01–13, JC01–14, and JC01–15 were recovered from broken margin (Fig. 2a).

The lherzolite samples (JC04–1 to JC04–4) from elevation 934 m consist of olivine (50–70 vol%), clinopyroxene (10–15 vol%), orthopyroxene (10–15 vol%), and plagioclase (2–5 vol%), with minor phlogopite, hornblende and chromite. Olivine is anhedral and commonly enclosed by interstitial clinopyroxene or orthopyroxene grains. The sulfide-disseminated lherzolite samples corresponding to the disseminated ores (JC01–1 to JC01–5; JC01–11 to JC01–15; JC01–19 to JC01–23; JC03–33 to JC03–38) were recovered at 1018 m and 934 m levels. They contain 60–85 vol% olivine, 10–30 vol% pyroxene (clinopyroxene > orthopyroxene), 5–10 vol% sulfide, 5–10 vol% hornblende, and 5–10 vol% phlogopite, with minor chromite which occurs as interstitial grains or as small inclusions in olivine. The rest of the samples are the sulfide-(patchy) net-textured dunites corresponding to the (patchy) net-textured ores. They contain 60–80 vol% olivine, 15–40 vol % sulfide, and 1–8 vol% pyroxenes (clinopyroxene > orthopyroxene) with minor phlogopite, apatite, hornblende, and chromite crystals.

3.2. Analytical methods

Textural and mineralogical investigations were conducted using TM4000plus scanning electron microscopy system equipped with Bruker Quantax 75 energy-dispersive spectroscopy at the Institute of Geology and Geophysics, Chinese Academy of Sciences (IGGCAS). Back-scattered electron (BSE) images were obtained at an accelerating voltage

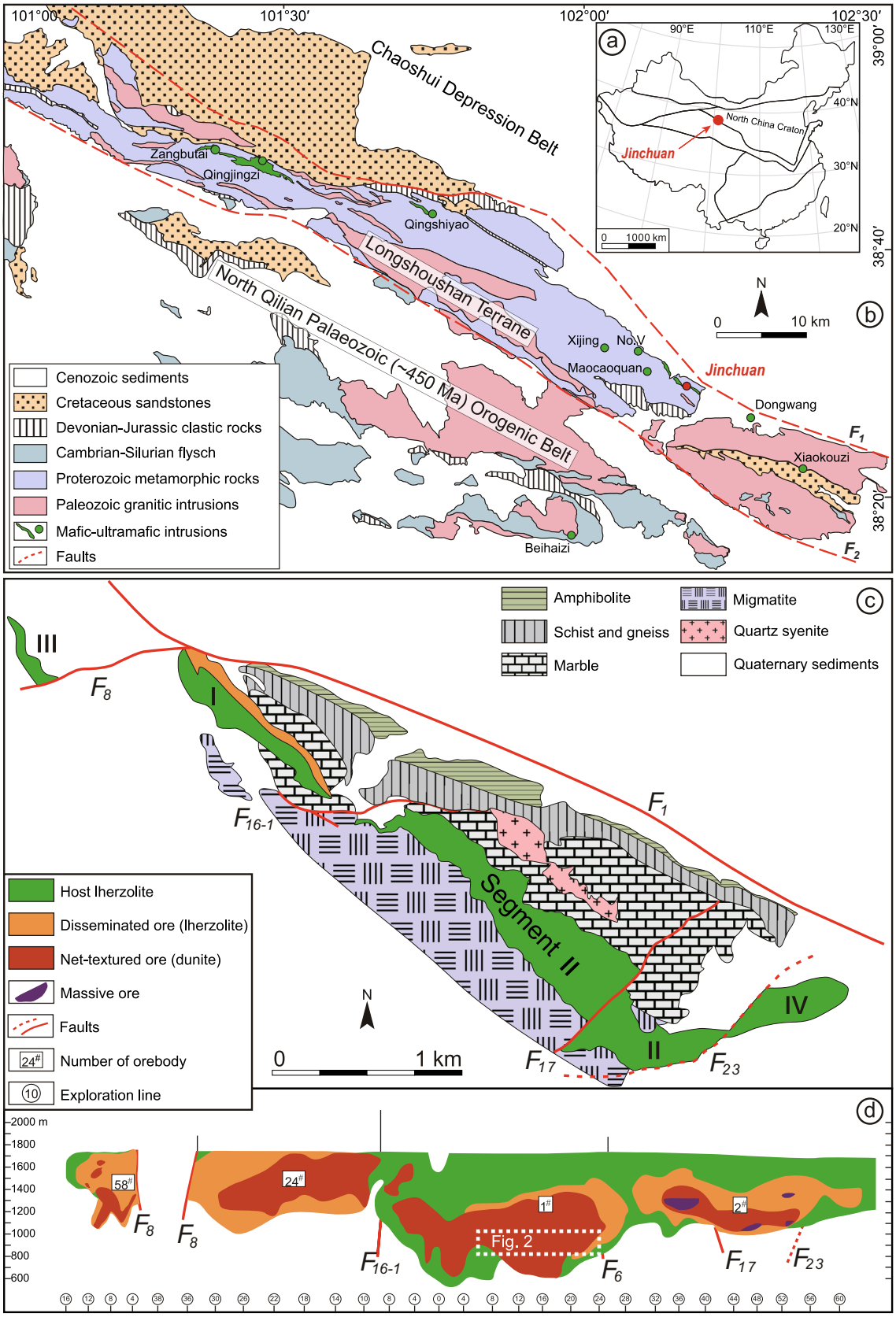

Fig. 1. (a) Tectonic units of China. (b) Simplified regional geological map of the Longshoushan Terrane (modified after Li and Ripley, 2011 and Duan et al., 2015). (c-d) Geological map and longitudinal section of the Jinchuan deposit (modified after Song et al., 2012).

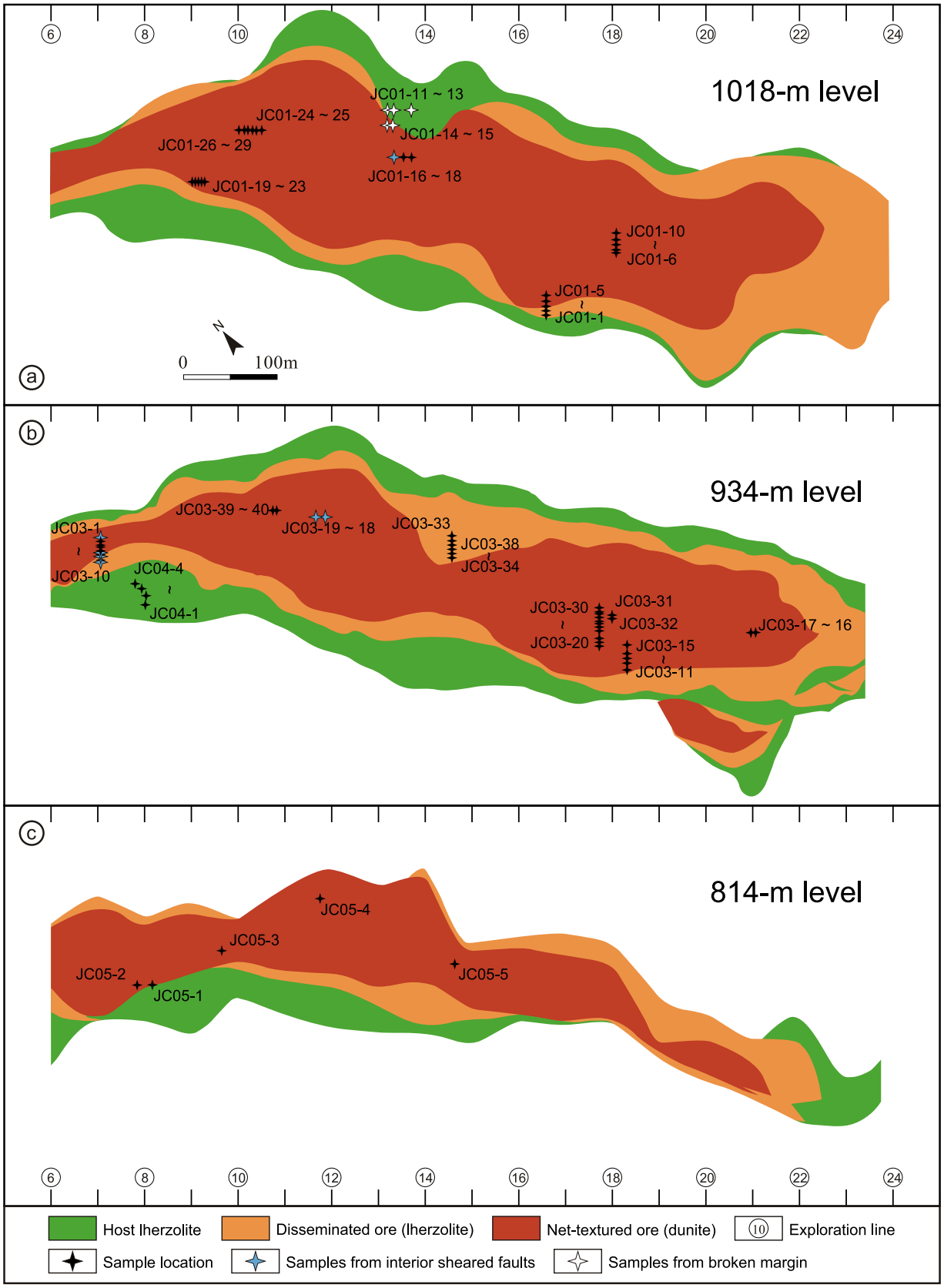

Fig. 2. Selected geological maps of Orebody 1 in Segment II and sample locations at elevations of (a) 1018 m, (b) 934 m, and (c) 814 m.

of 15 kV and 20 kV to illustrate texture and alteration features between sulfide aggregates and silicate minerals. Semi-quantitative chemical analyses were used to identify minerals at 20 kV accelerating voltage. The acquisition time of each spot was 15 s, ensuring the spectrum area exceeded 2.5×10^5 counts.

In-situ major element compositions of minerals were determined on thin sections using a JEOL JXA8100 electron probe microanalyzer (EPMA) at IGGCAS. The analytical conditions were accelerating voltage of 15 kV, 10 nA beam current, 5 μm beam spot and 10–30 s counting time on peak. Natural and synthetic minerals were used for standard calibration, and a program based on the ZAF procedure was used for matrix corrections. Analytical uncertainties for all elements analyzed were better than 1–2%.

In-situ trace element analyses of olivine were conducted on thin sections using a 193 nm Coherent GeoLasPro ArF Excimer laser coupled to an Element XR, Thermo Fisher inductively coupled plasma mass spectrometer (LA-ICP-MS) at IGGCAS. Prior to LA-ICP-MS analysis, thin sections previously coated with carbon for EPMA analyses were treated with 3% HNO_3, followed by de-ionized water and ethylene to clean the surfaces. Each analysis was performed using 44 μm diameter ablating spots at 5 Hz with an energy of ~100 mJ per pulse for 40 s after measuring the gas blank for 20 s. Standard reference materials NIST610 and NIST612 were used as external standards to produce calibration curves. Raw data processing was carried out offline using GLITTER 4.0 program.

4. Results

4.1. Post-magmatic modification features in the Jinchuan deposit

In this section, we recognize and describe typical post-magmatic hydrothermal alteration imprinted on the sulfide-bearing rocks with the aid of cracks that might serve as pathways of external fluids at varying scales.

The samples collected from highly sheared faults in the Orebody 1 (Fig. 2a-b) are sulfide-net-textured dunites. They have experienced the most pronounced hydrous alteration (Fig. 3a-d), especially confined sample margins with metallic coloration (Fig. 3a, b). In these samples, the original serpentine mesh texture has been totally overprinted by shear zones, and all silicate phases are completely serpentinized and have indistinct grain boundaries. There are remnants of chromite inclusion mostly rimmed by altered Cr-magnetite (Fig. 3c). Net-textured

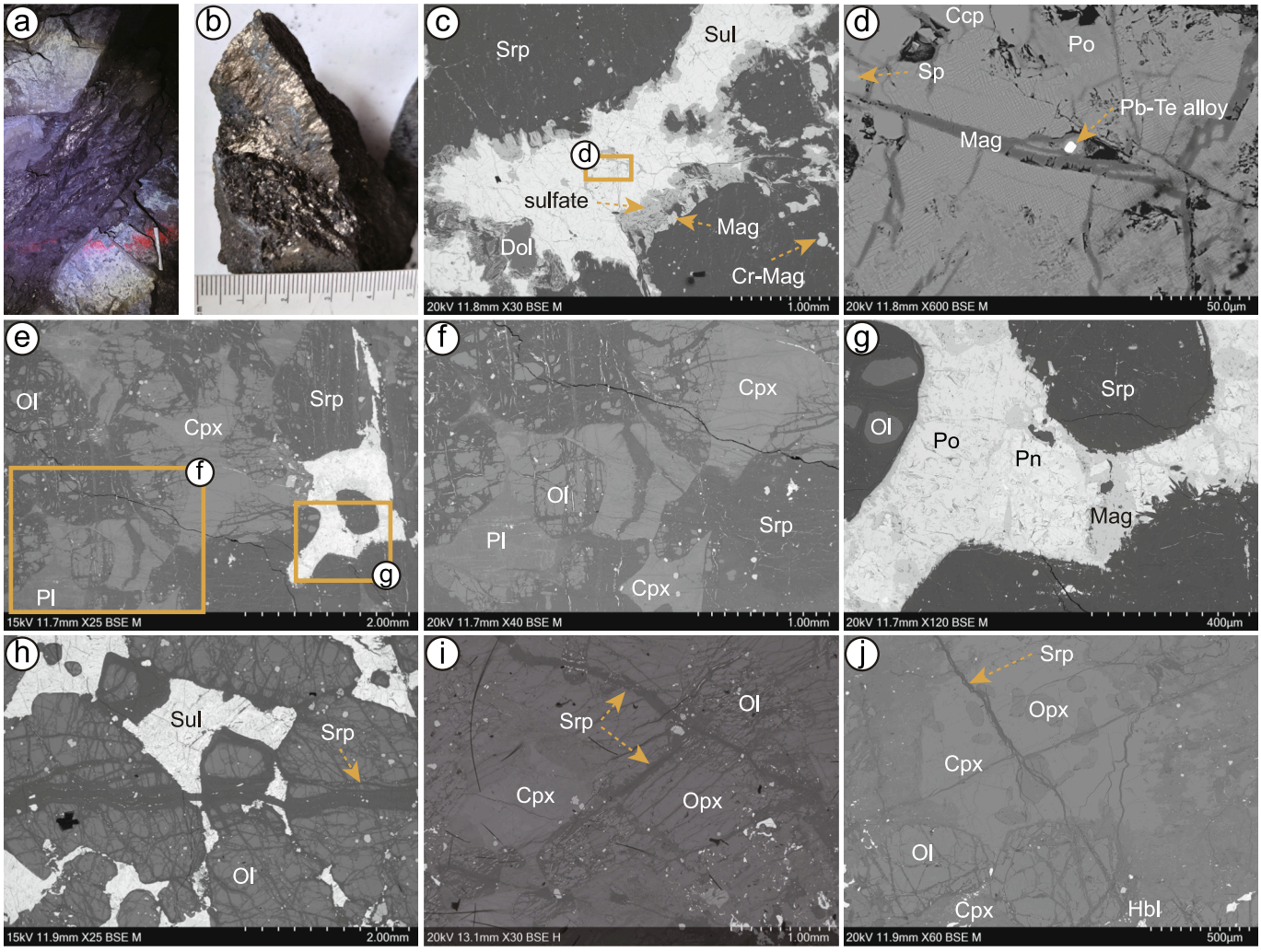

Fig. 3. Representative microphotographs of the post-magmatic alteration of samples from Orebody 1 in the Jinchuan deposit. (a-c) Net-textured samples from sheared-fractures infillings are replaced completely by serpentine, magnetite and sulfate with occurrences of dolomite and (d) sphalerite and Pb-Te alloy. (e) Samples from the broken margin of orebody show heterogeneous hydrothermal alteration of (f) silicate minerals and (g) sulfide minerals. (h-j) Samples from the interior of the orebody are crosscut by microfractures and exhibit limited hydrothermal alteration centered on the fractures. Abbreviations: Ol, olivine; Cpx, clinopyroxene; Opx, orthopyroxene; Hbl, hornblende; Pl, plagioclase; Srp, serpentine; Sul, sulfide; Po, pyrrhotite; Pn, pentlandite; Ccp, chalcopyrite; Sp, sphalerite; Mag, magnetite; Ilm, ilmenite; Dol, dolomite.

sulfides are commonly replaced by Fe-oxide or Fe-sulfate occurring as irregular rims on sulfide aggregates (Fig. 3c). Pb-Te alloy and sphalerite are occasionally present (Fig. 3d).

The samples recovered from broken margin of the orebodies (Fig. 2a) also display heterogeneous hydrothermal alteration (Fig. 3e-g). Their silicate minerals are partially or completely altered (Fig. 3e, f), whereas most sulfide aggregates have fresh interior and are surrounded by thin magnetite rims (Fig. 3e, g) that may have resulted from self-oxidization or alteration of adjacent silicate minerals. Other samples are occasionally penetrated by millimeter-scale micro-fractures and display veinlet hydrothermal alteration centered on the micro-fractures, but generally, the majority remain unblemished by hydrothermal activity (Fig. 3h-j).

These post-magmatic modifications of sulfide-bearing rocks are spatially concentrated along the cracks (Fig. 3). The modifications are spatially heterogeneous and have no defined distribution at orebody-scale. It effectively modified the chemical compositions of the primary silicate minerals (Fig. 3c, e-j) and destroyed the original mesh texture in olivine (Fig. 3c, e, g, h) and cumulus texture of the rocks (Fig. 3e-f, i-j).

The primary sulfide minerals are also vulnerable to the post-magmatic modifications. The sulfide aggregates are cross-cut by micro-fractures (Fig. 3h) and rimmed by secondary magnetite and/or sulfate (Fig. 3c, e, g). Petrographically, the most identifiable features of post-magmatic modifications are the spatial heterogeneity of overprinting on the original mesh texture (Fig. 3c, e-j) and secondary oxide and/or sulfate around sulfide aggregates (Fig. 3c, e, g).

4.2. *Alteration features of olivine dependence on sulfide contents*

In the net-textured ores containing 30–40 vol% sulfide, serpentinization of cumulus olivine is commonly pervasive, but the continuum of sulfide minerals enclosing cumulus olivine remain unaffected by hydrothermal alteration (Fig. 4a, b). Relict olivine occurs as islands within serpentine mesh texture (Fig. 4b). In most cases, the percentages of serpentine plus magnetite are equal to or higher than those of the remaining olivine (Fig. 4b). Notwithstanding the high serpentinization intensity of the cumulus olivine, the olivine-sulfide interfaces are regular

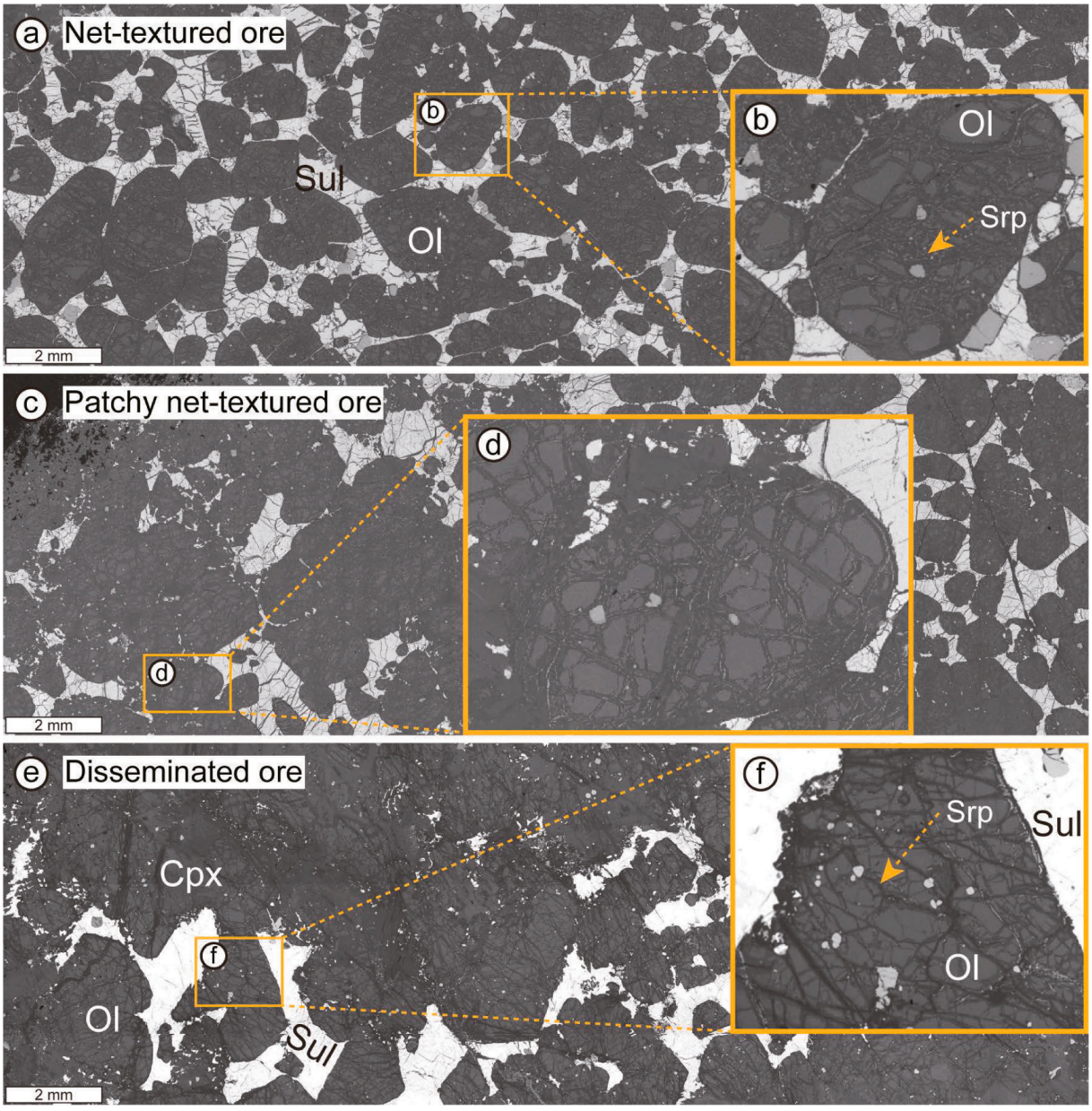

Fig. 4. Back-scattered electron (BSE) images showing representative alteration features of decreasing alteration intensity with decreasing sulfide contents from (a-b) net-textured ore through (c-d) patchy net-textured ore to (e-f) disseminated ore at orebody-scale.

and smooth in the samples (Fig. 4a, b).

In the patchy net-textured ores containing 10–30 vol% sulfide, the serpentinization is extensive (Fig. 4c, d) but the degree is lower than that in the net-textured ores (Fig. 4a, b). The discontinuous sulfide minerals around the altered olivine grains remain fresh (Fig. 4d). The percentages of serpentine plus magnetite are commonly less than those of relict olivine (Fig. 4d).

In the disseminated ores containing 5–10 vol% sulfide, the serpentinization intensity is generally lower (Fig. 4e, f) than that in the net-textured ores (Fig. 4a, b) and patchy net-textured ores (Fig. 4c, d) and the disseminated sulfide minerals remain unaffected by hydrothermal alteration (Fig. 4e, f). The serpentine and magnetite present along the intra-grain fractures and grain boundaries, and the percentages of serpentine plus magnetite are significantly less than those of the relict olivine (Fig. 4f).

The above systematic decline in the degree of serpentinization from net-textured ores, through patchy net-textured ores, to disseminated ores at orebody-scale (Fig. 4) indicates a dependence of alteration intensity on the sulfide contents. At thin section-scale, the olivine grains occurring in the sulfide-rich part are consistently characterized by higher degree of alteration intensity than those in the sulfide-barren part (Fig. 5).

4.3. Alteration features of olivine dependence on olivine-sulfide texture

There are two types of contact relationship between olivine and sulfide in the sulfide-bearing rocks: Type I, olivine is partially in contact with the sulfide aggregates; Type II, olivine is exclusively enclosed by sulfide aggregates (Fig. 6). In Type I, there is an envelope of serpentine around olivine at the olivine-sulfide interface (Fig. 6a). The Type I olivine displays decreasing serpentinization intensity from the olivine-sulfide interface to the core (Fig. 6a). In Type II, irregular patches of serpentine formed by replacement of olivine are restricted along the olivine-sulfide interface. The portions abutting other olivine grains are less serpentinized than those adjacent to the sulfide aggregates. No obvious relationships between the serpentinization intensity and the interstitial sulfide species in the studied samples can be observed (Fig. 7). The above-mentioned alteration features show that the degree of serpentinization decreases along the distance far away the sulfide aggregates (Fig. 6) and has no dependence on the sulfide species (Fig. 7). Similar alteration features are shown in Fig. 5b as well.

4.4. Alteration features of olivine dependence on hydrous minerals

The pristine hydrous minerals occur as fine-grained interstitial phases and make up <10 vol% of the sulfide-bearing rocks. Intergrown textures of hydrous minerals, sulfide minerals and pyroxenes are pervasively developed (Fig. 8). In Fig. 8a, the mere presence of phlogopite and hornblende on the right of the sulfide aggregates. The uneven distribution of hydrous minerals causes the olivine grains on the same side to display lower alteration intensity in the interior of the olivine and along the olivine-sulfide interface compared to olivine grains on the other side of sulfide aggregates (Fig. 8a). In Fig. 8b, when individual olivine grain sandwiched between hornblende (left) and sulfide (right), the serpentinization intensity at the olivine-hornblende interface is much lower than that at the olivine-sulfide interface. The above discrepancies in alteration intensity suggest that the presence of the hydrous minerals would protect the adjacent olivine grains from serpentinization (Fig. 8).

4.5. Olivine compositional variations

Major element compositional profiles determined by EPMA are listed in Table S1. The olivine grains in the net-textured ores have a wide range of intra-grain Fo contents, ranging from 79.7 to 85.2, but the variation of Fo content in individual olivine grain is essentially <2. In the olivine grains with Fo contents higher than 82 from net-textured ores, the compositional zoning profiles of Fo and Ni are commonly observed. The Fo and Ni decrease from the core of olivine to the rim in contact with sulfide (Table S1; Fig. 9a-b). The olivine grains with medium Fo contents (80–82) from the net-textured ores exhibit relatively scattered distributions in Fo and Ni contents (Table S1; Fig. 9c-d). In the olivine grains (Fo = 79.2–82.6) from the patchy net-textured ores, no Fo content zoning has been observed (Table S1; Fig. 9e-h) especially in olivine with Fo content of Fo82 (Fig. 9e) and Fo80 (Fig. 9h). We note that Fig. 9f shows an asymmetrical variation in Fo content zoning profiles in olivine grain. The olivine grain rim adjacent to the sulfide displays an immediately sharp decrease in Fo contents but the part in contact with orthopyroxene is homogenous (Table S1; Fig. 9f). The intra-grain Ni contents show no systematic variation with varying Fo contents (Table S1; Fig. 9e-h). The olivine grains from disseminated ores have intra-grain Fo contents range from 79.8 to 83.8 (Table S1; Fig. 9i-k). The olivine grains have trends to approach Fo82 at the rims in contact with interstitial silicate minerals and scattered Ni distributions at grain-scale (Fig. 9i, k). An exception is in Fig. 9j, which shows the relative homogeneity in Fo contents but Ni contents systematically decrease from the core to the rim.

In comparison to the ores, the olivine grains in the sulfide-free lherzolite bordering clinopyroxene have highly variable Fo contents from 76.6 to 81.8 (Table S1; Fig. 9l). The intra-grain elemental distribution shows no chemical zoning from the core to the rim (Fig. 9l). In summary, the intra-grain profiles indicate that the general heterogeneity in Fo and Ni contents of olivine occurs both at grain- and orebody-scale. The individual olivine grains from sulfide-bearing rocks have relatively narrow ranges of Fo contents and remarkable zoning patterns in Fo and Ni contents from the core to the rim (Fig. 9a-k). In contrast, the individual olivine grains from the sulfide-free lherzolite span lower and wider range of Fo contents (up to 6) without apparent compositional

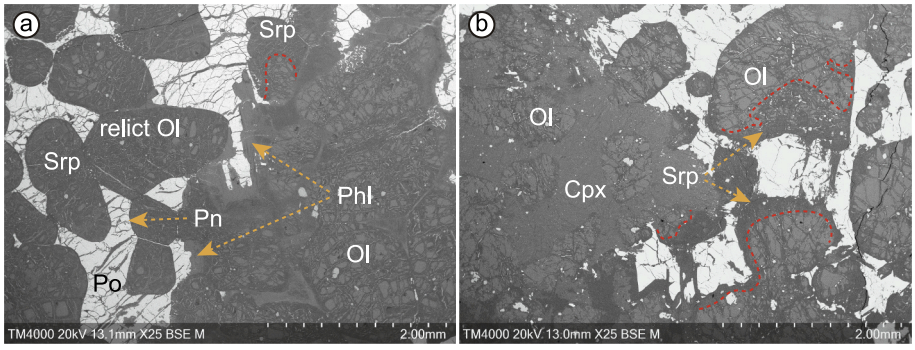

Fig. 5. The BSE images showing representative alteration features of olivine affected by sulfide contents at thin section-scale. (a) Olivine grains at the left sulfide-rich part are more serpentinized than that at the right sulfide-poor part. (b) Olivine grains isolated from sulfide at the right part are more serpentinized than that isolated from clinopyroxene at the left part. Abbreviations: Phl, phlogopite and others are same as Fig. 3.

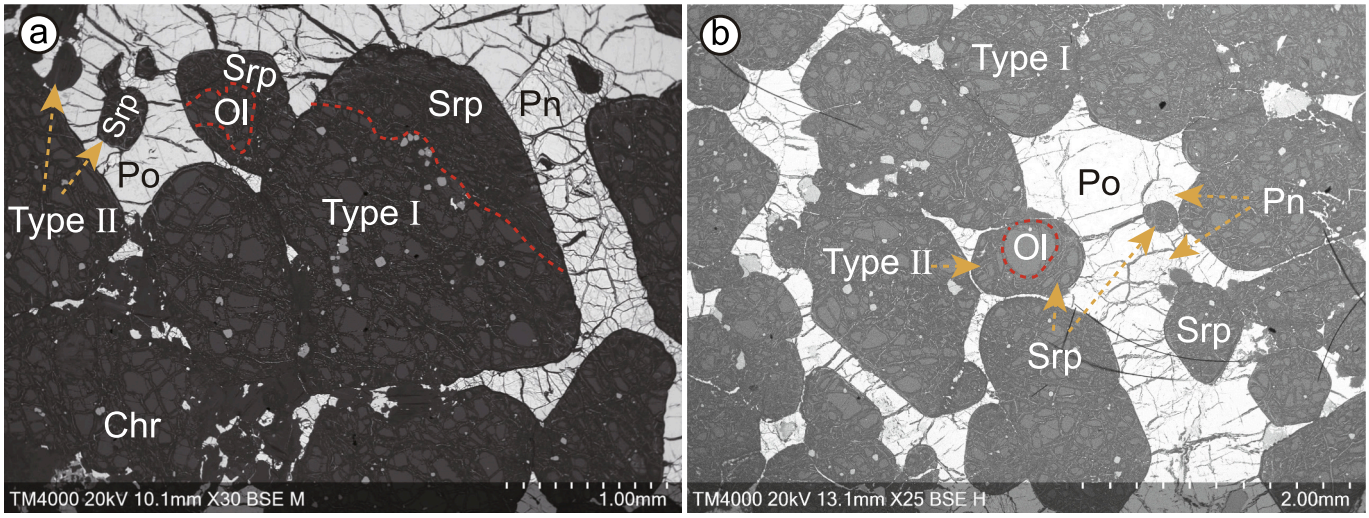

Fig. 6. BSE images showing representative alteration features in different olivine-sulfide texture. (a) The completely serpentinized Type I olivine and partially serpentinized Type II olivine. (b) Serpentinization of Type I olivine along the olivine-sulfide interface. Abbreviations: Chr, chromite and others are same as Fig. 3.

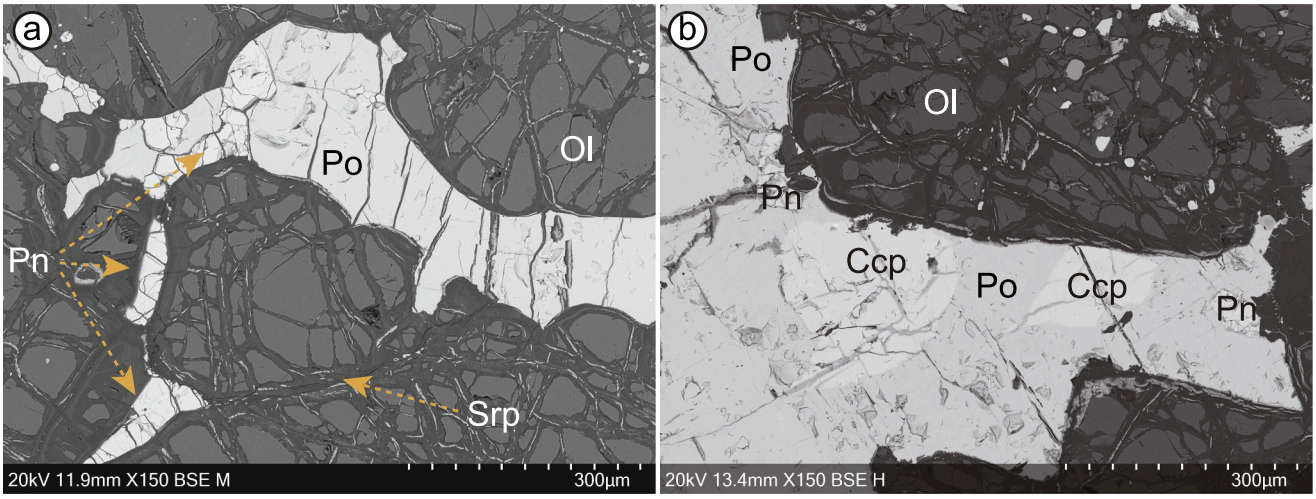

Fig. 7. BSE images showing representative alteration features of olivine affected by different sulfide minerals.

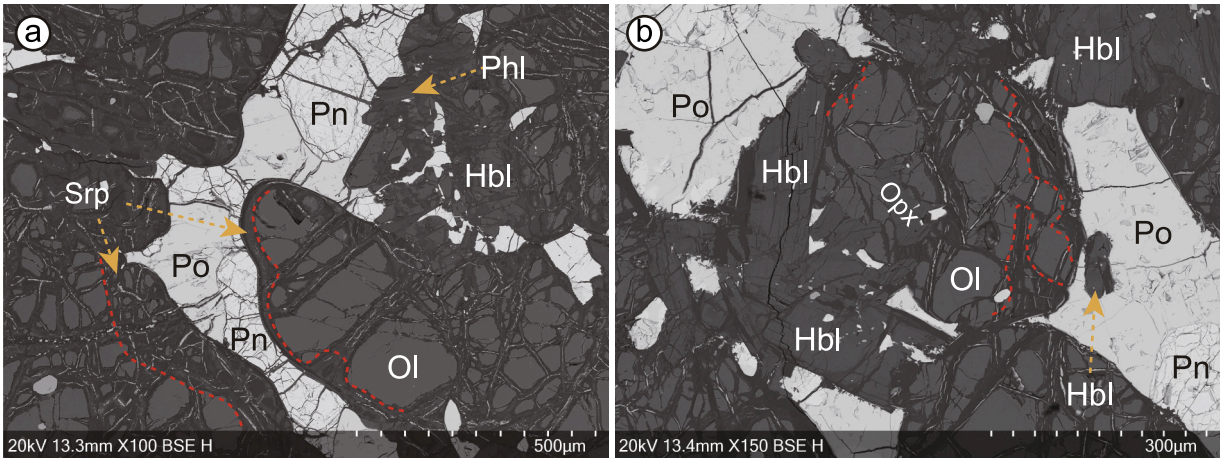

Fig. 8. BSE images showing representative alteration features of olivine affected by phlogopite and hornblende.

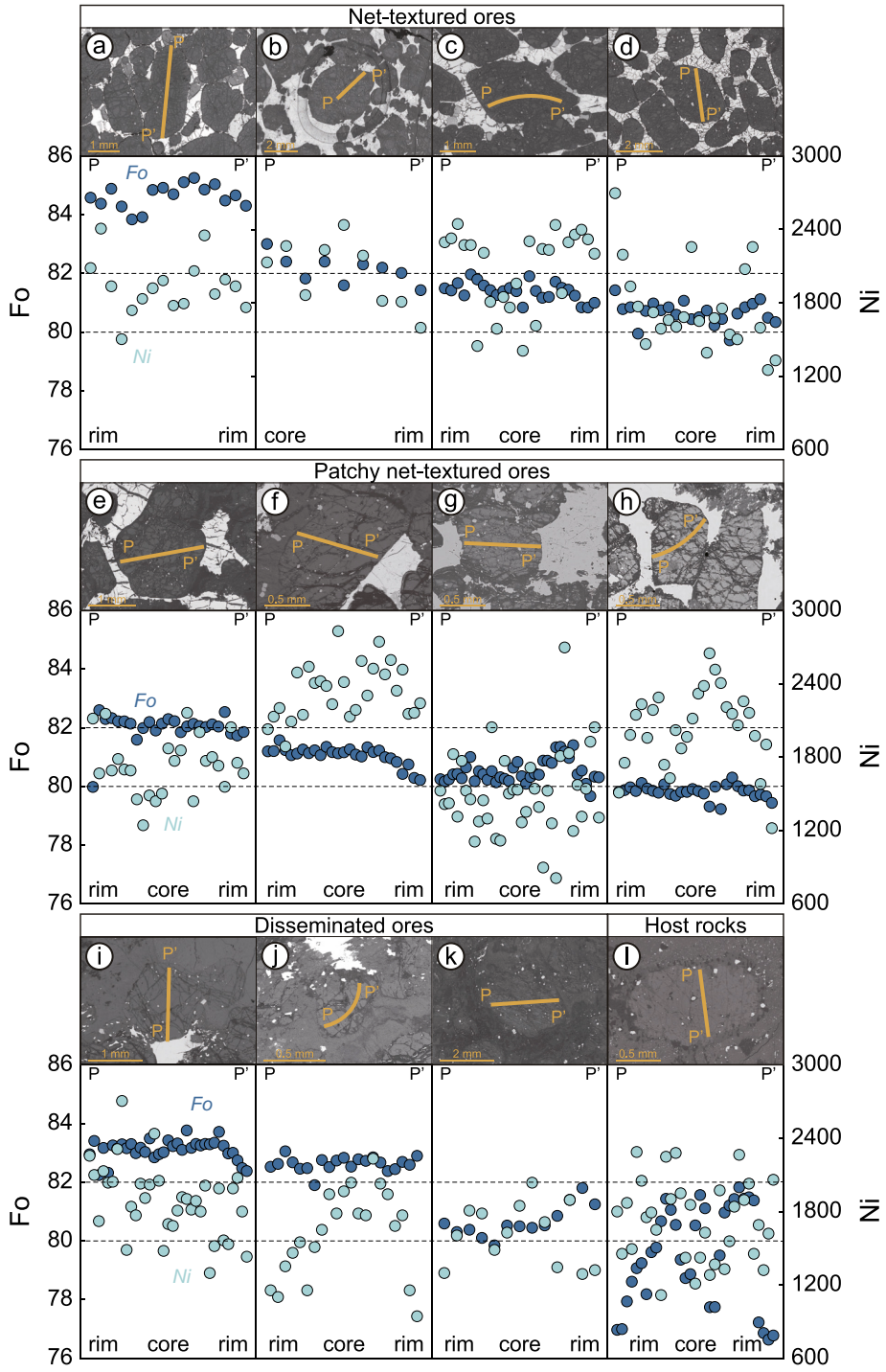

Fig. 9. BSE images and compositional profiles of Fo contents and concentrations of Ni in representative olivine determined by EPMA. Olivine grains from (a-d) sulfide-net-textured dunites, (e-h) sulfide-patchy net-textured dunites, (i-k) sulfide-disseminated lherzolites and (l) sulfide-free lherzolite. Each intra-grain profile starts from P and ends at P′.

gradients in Fo contents (Fig. 9l).

Trace element compositional profiles of olivine determined by LA-ICP-MS are listed in Table S2. The olivine grains in the net-textured ores are relatively higher in Ni (1925–2467 ppm) concentrations and Ni/Co ratios (10.2–15.3), and lower in Mn (1549–1886 ppm) and Co (136–193 ppm) concentrations (Fig. 10a-b) than those in the host lherzolite (Mn 1806–2506 ppm, Co 178–222 ppm, Ni 1536–1840 ppm, Ni/Co 7.32–10.3; Fig. 10c). They show symmetric reverse zonings in terms of Ni (Ni-poor cores, Ni-rich rims) and Co (Co-rich cores, Co-poor rims) (Fig. 10a-b). However, the normal zoned olivine grain in the host lherzolite shows Co enrichment and Ni depletion in the rims (Fig. 10c).

In the lherzolite-hosted olivine, Mn contents have negative correlations with Ni contents and Ni/Co ratios but positive correlation with Co contents (Fig. 10f). These relationships are reversed in the olivine in net-textured ores containing hydrous minerals, in which Mn contents are positively correlated with Ni contents and Ni/Co ratios but negatively correlated with Co (Fig. 10d). No correlations between Ni/Co ratios, Mn and Ni contents can be observed in the olivine grains from hydrous minerals-poor ores (Fig. 10e).

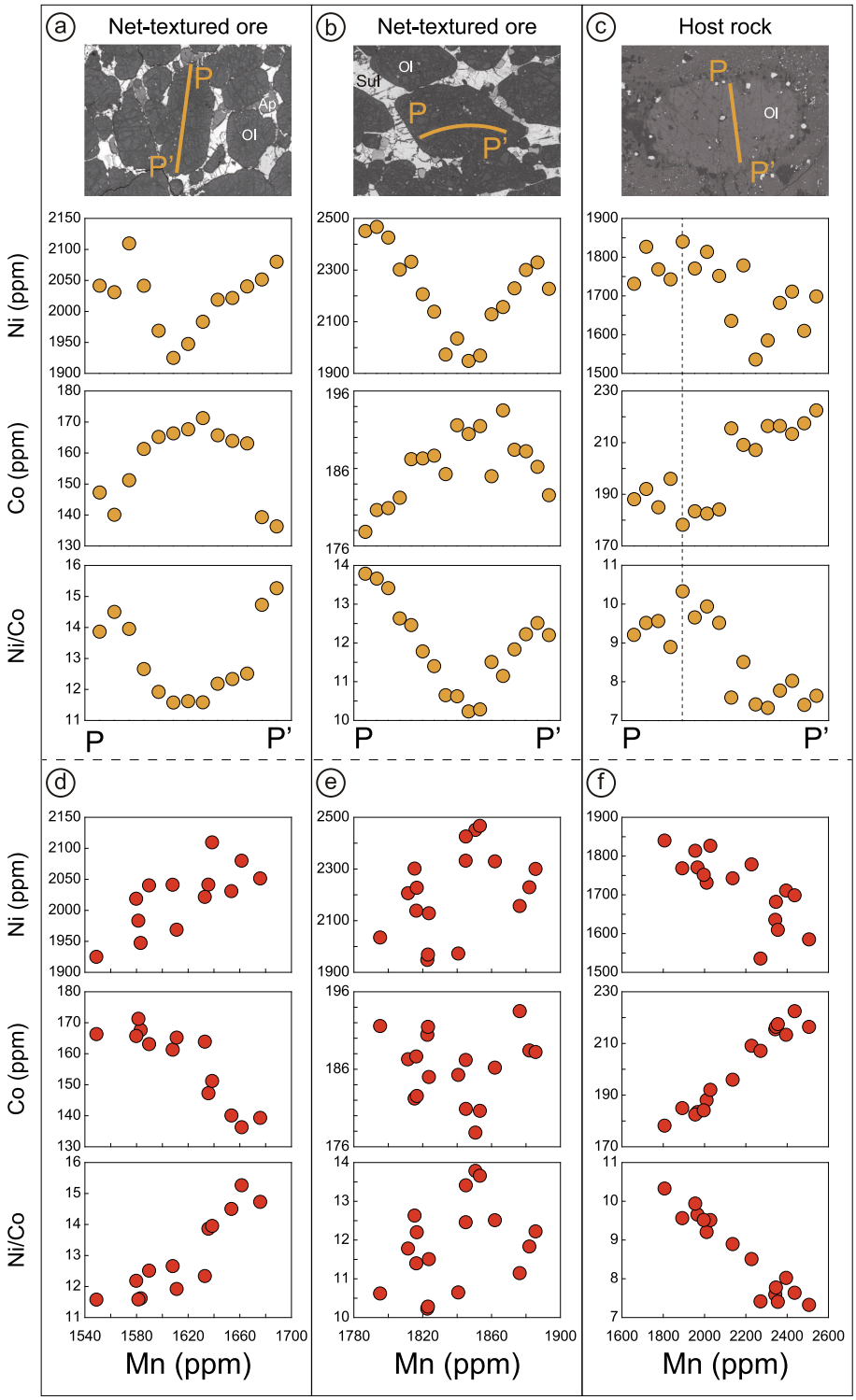

Fig. 10. BSE images and Mn-Ni-Co-Ni/Co covariations in representative olivine grains determined by LA-ICP-MS. (a-b) Reverse zonings of Ni, Co and Ni/Co ratio in olivine from sulfide-net-textured dunites. (c) Normal zoned olivine crystal from sulfide-free lherzolite. Correlations of Mn with Ni, Co and Ni/Co ratio in olivine from (d) hydrous mineral-rich net-textured ore and (e) hydrous mineral-poor net-textured ore that contrary to (f) sulfide-free lherzolite.

5. Discussion

5.1. *Selective alteration relevant to post-magmatic hydrothermal alteration or syn-mineralization?*

Previous studies on the post-magmatic modifications of the magmatic sulfide deposits have described the development of low-temperature water-rock processes (e.g., Li et al., 2004a, 2008) and remobilization of metal elements (e.g., Farrow and Watkinson, 1996; Lightfoot et al., 2017; Liu et al., 2016; Mansur et al., 2021). The Jinchuan deposit has long been thought to have suffered intensive post-magmatic modifications (Ripley et al., 2005), which resulted in the secondary addition of a wide variety of hydrous minerals including serpentine, tremolite, actinolite, talc, and chlorite (Chai and Naldrett,

1992; Barnes and Tang, 1999; Li et al., 2004a; Ripley et al., 2005; Song et al., 2012) as well as platinum-group elements mineralization (Prichard et al., 2013; Yang et al., 2006; Yang et al., 2018). In the studied samples from the Jinchuan deposit, the post-magmatic modifications of sulfide-bearing rocks are observed being focused along the cracks at varying scales from thin section to orebody (Fig. 3) and petrographically overprinted on the original mesh texture in olivine (Fig. 3c, e-j). The rim of sulfide aggregates has been oxidized to secondary magnetite (Fig. 3c, e, g).

The selective alteration, proposed in podiform chromite deposits (Su et al., 2020) and Hongqiling Ni-Cu deposit (Cui et al., 2022), in the Jinchuan deposit displays distinct petrographic features with post-magmatic hydrothermal alteration. It is characterized by systematic serpentinization of the original olivine in association with pristine sulfide at varying scales (Figs. 4-8). The objects constitute the selective alteration including cumulus olivine, sulfide aggregates, primary hydrous minerals (phlogopite, apatite, and hornblende), with original mesh-textured olivine grains in the Jinchuan deposit. The degree of selective alteration is dictated by the sulfide contents (Figs. 4-5), olivine-sulfide textures (Fig. 6), and the occurrence of interstitial hydrous minerals (Fig. 8). The post-magmatic alterations locally modified the chemical composition of the silicate minerals and the sulfide minerals.

Both the post-magmatic and selective alteration involve the introduction of hydrous fluids (Cui et al., 2022). If the hydrous fluids were derived from external sources postdating the mineralization processes, the alteration would yield two kinds of results: (1) at orebody-scale, the alteration intensity would decrease progressively inward to the center of the intrusion (Ripley et al., 2005); (2) at thin section-scale, the interstitial anhydrous silicate phases such as pyroxene enclosing the olivine would also be altered (Fig. 3e-f, i-j). However, the selective alteration shows alteration intensity increase inward to the core at orebody-scale (Fig. 4) indicating the alteration results from syn-mineralization hydrous fluids. Furthermore, the hydrous minerals, intergrown with the interstitial sulfide and pyroxenes, can lower the degree of selective alteration (Cui et al., 2022), suggesting that the hydrous minerals formed during syn-mineralization fluid activity as well.

In the Jinchuan deposit, the decrease of $\delta^{18}O$ values of the olivine as the increase of degree of the serpentinization (Ripley et al., 2005) may suggest the equilibrium between olivine, serpentine and water reached. The higher $\delta^{18}O$ values of the olivine than serpentine (Ripley et al., 2005) therefore indicate the mineral/water oxygen fractionation factor of olivine is higher than serpentine. Since the mineral/water oxygen fractionation factor is a function of temperature (Vho et al., 2019), the serpentinization of olivine require high-temperature (Vho et al., 2019) that are consistent with magmatic temperature (Bindeman, 2008).

5.2. *Direct origin, role, and fate of hydrous fluids in the Jinchuan Ni-Cu sulfide deposit*

Hydrous fluids with high content soluble volatiles play a critical role in magma transportation and ore-forming process. During the ascent of the ore-bearing high-Mg parental basaltic magmas, exsolution of volatiles would cause gas bubble nucleation, growth, and possible coalescence (Métrich and Wallace, 2008; Mungall, 2015; Yao and Mungall, 2020). The vapor bubble is spontaneous attached to the stable sulfide phases to form the compound drops because of the surface tension (Botcharnikov et al., 2013; Mungall et al., 2015; Mungall and Brenan, 2014; Mungall and Su, 2005). The compound drops are evidenced by natural globular sulfide ore textures (e.g., Barnes et al., 2019; Barnes et al., 2020; Le Vaillant et al., 2017; Liu et al., 2010; Schoneveld et al., 2020) and numerical modeling (Chung and Mungall, 2009; Yao et al., 2019; Yao and Mungall, 2020). The attachment of sulfide droplets to low-density vapor bubble increases the ability of sulfide liquid to migrate upward to shallow metallogenic system (Edmonds, 2015; Le Vaillant et al., 2017; Mungall et al., 2015; Yao et al., 2019; Yao and Mungall, 2020).

The vapor bubbles that latched onto the sulfide droplets due to surface tension can be a potential candidate for the hydrous fluid activities happened in the Jinchuan deposit. When the compound drops rise to the shallow, the immiscible fluids released during the crystallization of sulfide minerals would penetrate into and hydrate the adjacent cumulus olivine, resulting in the selective alteration. The extent of fluid-olivine reaction would depend on the volume of fluids that dictates the upward migration of sulfide liquid suggesting that more sulfide minerals as intercumulus phases need more fluids to form low-density compound drops and subsequently released. In other word, the high content of sulfide can be an indicator of higher degree of hydrous fluid activity, which is analogous to the positive relationship between proportions of chromite and degrees of fluid activity in chromite deposits (Su et al., 2020, 2021). Therefore, the serpentinization of olivine generally increases with increasing modal abundance of interstitial sulfide minerals. This mechanism can be responsible for the unequal intensity of alteration between the olivine grains (Figs. 4, 5) as well as between the pristine interstitial pyroxenes and the serpentinized cumulus olivine (Figs. 3a, 5b). Since primary hydrous minerals can hold water in the crystalline structure, crystallization of small amounts of hydrous minerals would incorporate a portion of water in their structure (Su et al., 2020) and lower the fluids contents in the interstitial vapor-sulfide-silicate system. Therefore, the cumulus olivine grains immediately adjacent to the hydrous minerals would be less altered than those which are out of reach of uptake of fluids by hydrous minerals. In some instances, the olivine grains are petrographically protected from selective alteration by pristine hydrous minerals (Fig. 8). As shown above, part of the hydrous fluid released from sulfide liquid was involved in serpentinization, and another part was trapped in primary hydrous minerals. The process of serpentinization is isochemical for major elements (Si, Mg, Fe) in olivine, whereas minor and trace elements such as Ca, Al, Cr are supposed to lost to hydrous fluids (Shervais et al., 2005). Thus, the hydrous fluids became progressively enriched in Ca, Al, Cr which are favorable to the saturation of apatite and hornblende. Besides, the heterogeneity of chlorapatite in sulfide-bearing rocks and relative lower Ce anomalies (δCe) fluorapatite in lherzolite imply the reducing redox state (Liu et al., 2021) and enrichment of F as the hydrous fluids evolve.

Empirical and experimental olivine/liquid partition coefficients ($^{olivine/liquid}D$) suggest that growth of olivine would produce Ni decreasing from core to rim (Fig. 10c) and negative correlation between Ni and Mn (Fig. 10f) at grain-scale (e.g., Bédard, 2005; Hirschmann and Ghiorso, 1994). Co is a compatible element in olivine, but only constant to increasing Co in planetary olivine is observed because of the increasing $^{olivine/liquid}D_{Co}$ and decreasing Co concentrations in silicate melts (Fig. 10c; Papike et al., 1999; Herd et al., 2009). Thus, the growth of olivine would produce positive correlation of Co with Mn (solid line in Fig. 11b) and systematic decrease in Ni/Co (Fig. 10f). Therefore, the distributions of Ni (Ni-rich cores, Ni-poor rims), Co (Co-poor cores, Co-rich rims) and Mn (Mn-poor cores, Mn-rich rims) in normal zoned olivine from sulfide-free lherzolite (Fig. 10c, f) behave as expected for being consistent with the fractional crystallization model. The Fe-Ni exchange between olivine and sulfide liquid would produce a negative relationship between Fo and Ni contents in olivine (Fig. 11a; Li et al., 2003). As a result of the positive correlation between the exchange-coupled pair of elements (i.e., Fe-Ni pair), reverse zoning of Ni can be developed (Fig. 10a-b) and the original negative Fe-Ni correlation can be turned upside down (Fig. 11c). Moreover, the feasible Co-Ni exchange could also be developed in same samples. The reverse zoning with respect to Co (Fig. 10a-b) can be explained by Ni-Co exchange preceding Fe-Ni exchange owing to the dependence of Co to Ni. The inverse correlation between Mn and Co in olivine from sulfide-bearing rocks (dashed line in Fig. 11b) contrary to sulfide-free lherzolite (solid line in Fig. 11b) may indicate that Co migrates from olivine to sulfide liquid during sulfide liquid-olivine Ni-Co exchange (Fig. 11d).

Previous studies suggest that the Fe-Ni exchange between olivine and sulfide liquid is dependent on temperature, melts composition, oxygen

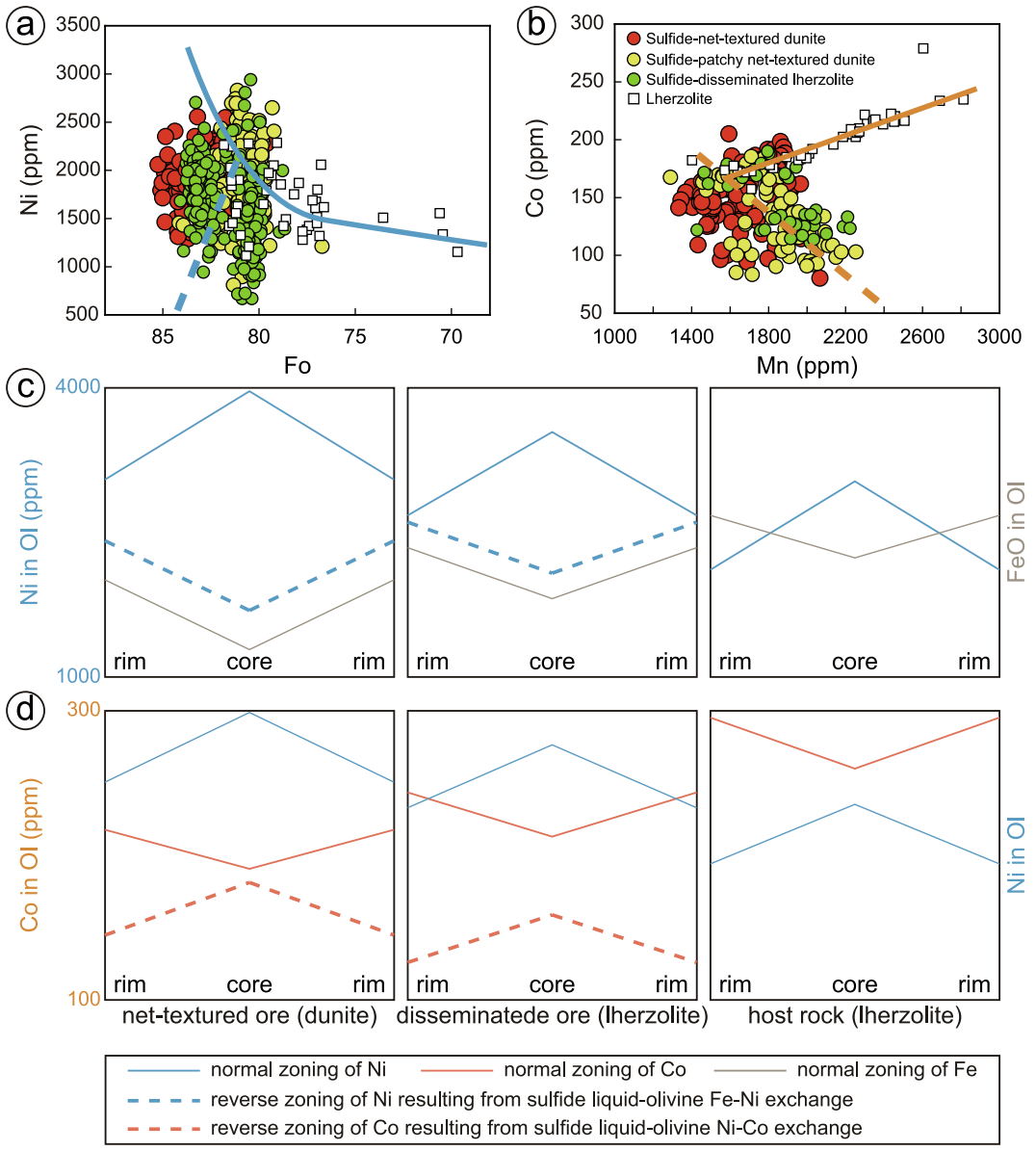

Fig. 11. Fractional crystallization (in solid line) and elemental exchange (in dashed line) curves of olivine. (a) Concave-up trend on a Fo-Ni diagram (in solid line) produced by fractional crystallization of olivine, and inverse Fo-Ni relationship (in dashed line) resulting from Fe-Ni exchange. (b) Positive correlation between Mn and Co in olivine (in solid line) from sulfide-free lherzolite, and negative correlation (in dashed line) from sulfide-bearing rocks. (c) Ni and (d) Co zonings as indicators of fractional crystallization model of olivine and elemental exchange model between olivine and sulfide liquid.

fugacity and sulfur fugacity (e.g., Barnes et al., 2013; Brenan, 2003). However, the significant correlations of Ni, Co and Ni/Co with Mn in olivine has been observed in net-textured ores with hydrous minerals (Fig. 10d), which has not been found in the hydrous minerals-poor net-textured ores (Fig. 10e). This suggests the effect of fluids on the elemental exchange process cannot be neglected. The fluids may serve as an agent for elemental exchange similar to the fluid-mediated elemental exchange between olivine and chromite in ophiolites (Su et al., 2021). The more fluid involves, the more completion the elemental exchange proceeds to, indicating the involvement of fluids enhanced the elemental diffusive efficiency between olivine and the intercumulus liquids. As mentioned above, a combination of fractional crystallization and sulfide liquid-olivine Fe-Ni exchange may have contributed to the overall variation of olivine compositions in the Jinchuan deposit, the involvement of fluids in the sulfide-bearing rocks cannot be ruled out.

5.3. Application in magmatic Ni-Cu sulfide deposits related to hydrous parental magma

Majority of the $\delta^{34}S$ values of the sulfide of the Jinchuan deposit range from −2 to +2 ‰ (Duan et al., 2016; Gao et al., 2022; Ripley et al., 2005), similar to that of the orogenic magmatic Ni-Cu sulfide deposits. Examples include Hongqiling ($\delta^{34}S$ = −2.2 to +0.9 ‰, Hao et al., 2014), Piaohechuan deposit ($\delta^{34}S$ = −0.5 to +1.0 ‰, Wei et al., 2019), Kalatongke ($\delta^{34}S$ = −1.86 to +1.74 ‰, Tang et al., 2020) in the Central Asian Orogenic Belt and many Ni-Cu deposits ($\delta^{34}S$ = −1 to +2.8 ‰, Papunen and Mäkelä, 1980) in the Kotalahti and Vammala belts in Finland. These values are close to the range characteristic of mantle-derived sulfur $\delta^{34}S$, which undermine the effect of external sulfur on the sulfide saturation. Yao et al. (2019) showed that at a pressure of 200 MPa, the anhydrous parental magma of Talnakh (Krivolutskaya et al., 2001) may carry <5 vol% sulfide liquid, whereas the hydrous magmas containing about 3–4 wt% H_2O (Plank et al., 2013) may carry >15 vol% sulfide liquid. This

indicates the very efficient collection of mantle-derived sulfide from appropriate volumes of magmas (Ripley and Li, 2013), especially the hydrous magmas. Previous studies demonstrate that the low-density sulfide-volatile compound drops can transport upward by flotation (Mungall, 2015; Yao et al., 2019; Yao and Mungall, 2020). This study proposes a model for the genesis of *syn*-mineralization selective alteration (Fig. 12) that may also exist in the orogenic magmatic Ni-Cu sulfide deposits for the existence of volatile.

In the metallogenic system, the fractionation of mafic-ultramafic parental magma would produce cumulus crystals and evolved melt that may then be squeezed into the shallow structural traps (Fig. 12a). Injection of a pulse of sulfide liquid would disturb the accumulated crystals and take up the intercumulus space (Fig. 12b). This process would ultimately lead to the formation of different sulfide-silicate textures depending on the intercumulus phases and their contents. The Ni-Co exchange and Fe-Ni exchange between sulfide liquid and olivine produced reverse zonings of Ni and Co in olivine (Fig. 10a-b). When the sulfide liquid starts to crystallize (Fig. 12c), the fluids attached to the sulfide liquid would be released because sulfide minerals are structurally incompatible with water. Subsequently, the hydrous fluids would hydrate the adjacent cumulus phases (mostly olivine in the Jinchuan deposit), giving rise to the selective alteration. Therefore, the more abundance of interstitial sulfide liquid would accompany the more hydrous fluids to float and subsequent be released. Thus, a decreasing order of sulfide contents from right to left in the Fig. 12d corresponds to decreasing degree of hydration of cumulus olivine. Meanwhile, the growth of pyroxenes from interstitial silicate melt would not be influenced by the fluid activity for their late crystallization sequence. Consequently, the interstitial pyroxenes would display less alteration than the enclosed cumulus olivine. The interstitial hydrous minerals show a close association with the sulfide minerals in the Jinchuan deposit. Their crystallization would structurally accommodate most of the water in the fluids (Su et al., 2020) through which the adjacent cumulus olivine grains become less altered (Fig. 8). Moreover, the involvement of hydrous fluids should have enhanced elemental exchange between olivine and sulfide liquid accounting for good correlations of Ni and Co with Mn in olivine (Fig. 10d).

From this model, the syn-mineralization fluid activity is believed to extensively modify the composition of cumulus olivine during the ore-forming stage. Therefore, the chemical and isotopic compositions of olivine should be interpreted with caution to infer the nature and origin of the parental magmas.

6. Conclusion

Detailed studies of the petrographic characteristics of hydrothermal alteration distinguished the post-magmatic modifications and syn-mineralization selective alteration overprint on the sulfide-bearing rocks of the Jinchuan Ni-Cu sulfide deposit. The post-magmatic modifications due to fracturing and externally sourced fluid activity is spatially heterogeneous without apparent regularity in distribution at orebody-scale. The post-magmatic modifications are identified by the spatial heterogeneity of destruction of the serpentine mesh texture. In contrast, the selective alteration is characterized by the mesh texture in olivine from the sulfide-bearing rocks of the Jinchuan deposit. The degree of selective alteration increases systematically toward the core net-textured dunite at orebody-scale, which embodies the positive correlation between the alteration intensity and sulfide contents. Moreover, the crystallization of the primary hydrous minerals would lower the alteration intensity. The fluids responsible for the selective alteration were derived directly from the sulfide surface and were instrumental in the upward migration of the sulfide liquid. The olivine grains in sulfide-bearing rocks are reversely zoned with respect to Ni (Ni-poor cores, Ni-rich rims) and Co (Co-rich cores, Co-poor rims) which can be interpreted by stages of sulfide liquid-olivine Ni-Co exchange and Fe-Ni exchange. The good correlations of Mn with Co and Ni in olivine from hydrous mineral-rich net-textured ores relative to hydrous mineral-poor net-textured ores show that the involvement of hydrous fluids enhance elemental diffusion between the olivine and sulfide liquid. Predictably, the selective alteration would also occur in other magmatic sulfide deposits related to hydrous parental magma.

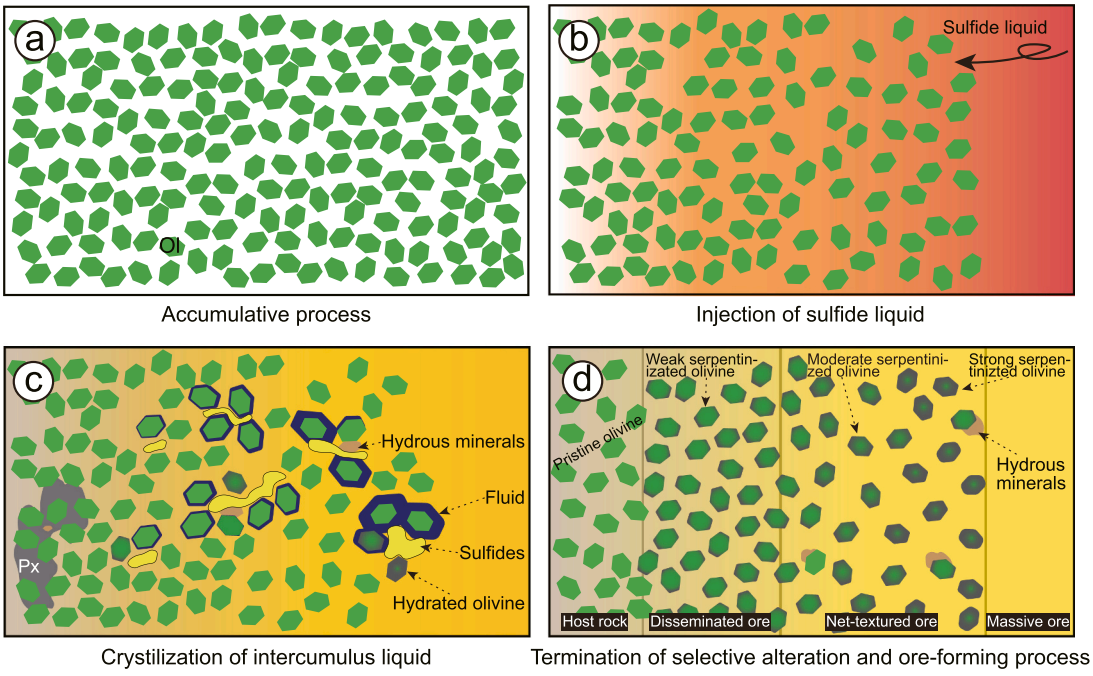

Fig. 12. A model showing the process of *syn*-mineralization selective alteration. (a) Olivine grains accumulate at the structural trap. (b) Sulfide liquid is injected into the trap, perturbates the accumulated crystals and takes up the intercumulus space. (c) Crystallization of sulfide minerals releases fluids that hydrate the adjacent cumulus olivine and mix with evolving melts to crystallize hydrous minerals. (d) Termination of metallogenesis and selective alteration.

Declaration of Competing Interest

The authors declare that there is no conflict of interest.

Data availability

The data supporting the findings of this study are included within Table S1 and Table S2 in the Supplementary materials.

Acknowledgements

This study was financially supported by project from the Ministry of Science and Technology National Key R&D Program of China (No. 2022YFC2903501) and Youth Innovation Promotion Association, Chinese Academy of Sciences. We appreciate the constructive reviews of two anonymous reviewers and editor Di-Cheng Zhu.

Appendix A. Supplementary data

Supplementary data to this article can be found online at https://doi.org/10.1016/j.lithos.2022.107014.

References

Barnes, S.J., Tang, Z.L., 1999. Chrome spinels from the Jinchuan Ni-Cu sulfide deposit, Gansu Province, People's Republic of China. Econ. Geol. 94, 343–356.
Barnes, S.J., Godel, B., Gürer, D., Brenan, J.M., Robertson, J., Paterson, D., 2013. Sulfide-olivine Fe-Ni exchange and the origin of anomalously Ni rich magmatic sulfides. Econ. Geol. 108, 1971–1982.
Barnes, S.J., Le Vaillant, M., Godel, B., Lesher, C.M., 2019. Droplets and bubbles: Solidification of sulphide-rich vapour-saturated orthocumulates in the Norilsk-Talnakh Ni-Cu-PGE ore-bearing intrusions. J. Petrol. 60, 269–300.
Barnes, S.J., Taranovic, V., Miller, J.M., Boyce, G., Beresford, S., 2020. Sulfide emplacement and migration in the Nova-Bollinger Ni-Cu-Co deposit, Albany-Fraser orogen, Western Australia. Econ. Geol. 115, 1749–1776.
Bédard, J.H., 2005. Partitioning coefficients between olivine and silicate melts. Lithos 83, 394–419.
Bindeman, I., 2008. Oxygen isotopes in mantle and crustal magmas as revealed by single crystal analysis. Rev. Mineral. Geochem. 69, 445–478.
Botcharnikov, R.E., Holtz, F., Mungall, J.E., Beermann, O., Linnen, R.L., Garbe-Schönberg, D., 2013. Behavior of gold in a magma at sulfide-sulfate transition: Revisited. Am. Mineral. 98, 1459–1464.
Brenan, J.M., 2003. Effects of fO_2, fS_2, temperature, and melt composition on Fe-Ni exchange between olivine and sulfide liquid: implications for natural olivine-sulfide assemblages. Geochim. Cosmochim. Acta 67, 2663–2681.
Chai, G., Naldrett, A.J., 1992. The Jinchuan ultramafic intrusion: Cumulate of a high-Mg basaltic magma. J. Petrol. 33, 277–303.
Chen, L.M., Song, X.Y., Danyushevsky, L.V., Xiao, J.F., Li, S.B., Guan, J.X., 2009. Correlation between Ni and MgO contents of olivine in Segment I of the Jinchuan intrusion, NW China, and its geological implication. Acta Petrol. Sin. 25, 3369–3378 (in Chinese with English abstract).
Chen, L.M., Song, X.Y., Keays, R.R., Tian, Y.L., Wang, Y.S., Deng, Y.F., Xiao, J.F., 2013. Segregation and fractionation of magmatic Ni-Cu-PGE sulfides in the western Jinchuan intrusion, northwestern China: Insights from platinum group element geochemistry. Econ. Geol. 108, 1793–1811.
Chung, H.Y., Mungall, J.E., 2009. Physical constraints on the migration of immiscible fluids through partially molten silicates, with special reference to magmatic sulfide ores. Earth Planet. Sci. Lett. 286, 14–22.
Cui, M.M., Su, B.X., Wang, J., Tang, D.M., Sakyi, P.A., Moynier, F., 2022. Linking selective alteration, mineral compositional zonation and sulfide melt emplacement in orogenic-type magmatic Ni-Cu sulfide deposits. J. Petrol. 63 egac043.
Dingwell, D., Romano, C., Hess, K.U., 1996. The effect of water on the viscosity of a haplogranitic melt under P-T-X conditions relevant to silicic volcanism. Contrib. Mineral. Petrol. 124, 19–28.
Duan, J., Li, C., Qian, Z.Z., Jiao, J.G., 2015. Geochronological and geochemical constraints on the petrogenesis and tectonic significance of Paleozoic dolerite dykes in the southern margin of Alxa Block, North China Craton. J. Asian Earth Sci. 111, 244–253.
Duan, J., Li, C., Qian, Z.Z., Jiao, J.G., Ripley, E.M., Feng, Y.Q., 2016. Multiple S isotopes, zircon Hf isotopes, whole-rock Sr-Nd isotopes, and spatial variations of PGE tenors in the Jinchuan Ni-Cu-PGE deposit, NW China. Mineral. Deposita 51, 557–574.
Duzhikov, O., Distler, V., Strunin, B., Sherman, M., Sluzhenikin, S., 1992. Copper-nickel sulfide ore-bearing formations: Geology and Metallogeny of Sulfide Deposits, Noril'sk Region, USSR. SEG Spec. Publ. 1, 61–146.
Edmonds, M., 2015. Research focus: Flotation of magmatic minerals. Geology 43, 655–656.
Farrow, C.E.G., Watkinson, D.H., 1996. Geochemical evolution of the Epidote Zone, Fraser Mine, Sudbury, Ontario; Ni-Cu-PGE remobilization by saline fluids. Explor. Min. Geol. 5, 17–31.
Gaetani, G.A., Grove, T.L., Bryan, W.B., 1993. The influence of water on the petrogenesis of subduction related igneous rocks. Nature 365, 332–334.
Gao, L.J., Long, T.M., Sun, D.Y., Deng, C.Z., Tian, Z.D., Song, X.Y., Yin, R.S., 2022. Crustal mercury addition into the giant Jinchuan Ni-Cu sulfide deposit, China, and its geological implications. Geochem. Geophys. Geosyst. 23 e2022GC010349.
Giordano, D., Russell, J.K., Dingwell, D.B., 2008. Viscosity of magmatic liquids: a model. Earth Planet. Sci. Lett. 271, 123–134.
Hao, L.B., Wu, C., Sun, L.J., Jiang, Y.M., Zhao, Y.Y., Lu, J.L., Li, J., 2014. Re-Os isotope characteristics of Hongqiling Cu-Ni sulfide deposit in Jilin Province and its significance. J. Jilin Univ. (Earth Sci. Ed.) 44, 507–517 (in Chinese with English abstract).
Herd, C.D., Dwarzski, R.E., Shearer, C.K., 2009. The behavior of Co and Ni in olivine in planetary basalts: an experimental investigation. Am. Mineral. 94, 244–255.
Hirschmann, M.M., Ghiorso, M.S., 1994. Activities of nickel, cobalt, and manganese silicates in magmatic liquids and applications to olivine/liquid and to silicate/metal partitioning. Geochim. Cosmochim. Acta 58, 4109–4126.
Hui, H., Zhang, Y., 2007. Toward a general viscosity equation for natural anhydrous and hydrous silicate melts. Geochim. Cosmochim. Acta 71, 403–416.
Krivolutskaya, N., Sluzhenikin, S., Turovtsev, D., Ariskin, A., 2001. Geochemical thermometry of rocks of the Talnakh intrusion: Assessment of the melt composition and the crystallinity of the parental magma. Petrology 9, 389–414.
Le Vaillant, M., Barnes, S.J., Mungall, J.E., Mungall, E.L., 2017. Role of degassing of the Noril'sk nickel deposits in the Permian-Triassic mass extinction event. Proc. Natl. Acad. Sci. 114, 2485–2490.
Lesher, C.E., Spera, F.J., 2015. Thermodynamic and transport properties of silicate melts and magma. In: The Encyclopedia of Volcanoes. Elsevier, pp. 113–141.
Li, C., Ripley, E.M., 2011. The giant Jinchuan Ni-Cu-(PGE) deposit: Tectonic setting, magma evolution, ore genesis, and exploration implications. Rev. Econ. Geol. 17, 163–180.
Li, C., Ripley, E.M., Naldrett, A.J., 2003. Compositional variations of olivine and sulfur isotopes in the Noril'sk and Talnakh intrusions, Siberia: Implications for ore-forming processes in dynamic magma conduits. Econ. Geol. 98, 69–86.
Li, C., Ripley, E.M., Merino, E., Maier, W.D., 2004a. Replacement of base metal sulfides by actinolite, epidote, calcite, and magnetite in the UG2 and Merensky Reef of the Bushveld complex, South Africa. Econ. Geol. 99, 173–184.
Li, X., Su, L., Song, B., Liu, D.Y., 2004b. SHRIMP U-Pb zircon age of the Jinchuan ultramafic intrusion and its geological significance. Sci. Bull. 49, 420–422 (in Chinese with English abstract).
Li, X.H., Su, L., Chung, S.L., Li, Z.X., Liu, Y., Song, B., Liu, D.Y., 2005. Formation of the Jinchuan ultramafic intrusion and the world's third largest Ni-Cu sulfide deposit: Associated with the ~825 Ma South China mantle plume? Geochem. Geophys. Geosyst. 6. Q11004.
Li, C., Ripley, E.M., Oberthür, T., Miller, J.D., Joslin, G.D., 2008. Textural, mineralogical and stable isotope studies of hydrothermal alteration in the main sulfide zone of the Great Dyke, Zimbabwe and the precious metals zone of the Sonju Lake Intrusion, Minnesota, USA. Mineral. Deposita 43, 97–110.
Lightfoot, P.C., Doherty, W., 2001. Chemical evolution and origin of nickel sulfide mineralization in the Sudbury Igneous Complex, Ontario, Canada. Econ. Geol. 96, 1855–1875.
Lightfoot, P.C., Naldrett, A.J., 1999. Geological and geochemical relationships in the Voisey's Bay intrusion, Nain plutonic suite, Labrador, Canada. In: Geological Association of Canada Short Course Notes, 13, pp. 1–30.
Lightfoot, P.C., Stewart, R., Gribbin, G., Mooney, S.J., 2017. Relative contribution of magmatic and post-magmatic processes in the genesis of the Thompson Mine Ni-Co sulfide ores, Manitoba, Canada. Ore Geol. Rev. 83, 258–286.
Liu, P.P., Qin, K.Z., Su, S.G., San, J.Z., Tang, D.M., Su, B.X., Sun, H., Xiao, Q.H., 2010. Characteristics of multiphase sulfide droplets and their implications for conduit-style mineralization of Tulargen Cu-Ni deposit, eastern Tianshan, Xinjiang. Acta Petrol. Sin. 26, 523–532 (in Chinese with English abstract).
Liu, Y.K., Mungall, J.E., Ames, D.E., 2016. Hydrothermal redistribution and local enrichment of platinum group elements in the Tootoo and Mequillon magmatic sulfide deposits, South Raglan trend, Cape Smith belt, New Quebec orogen. Econ. Geol. 111, 467–485.
Liu, M.Y., Zhou, M.F., Su, S.G., Chen, X.G., 2021. Contrasting geochemistry of apatite from peridotites and sulfide ores of the Jinchuan Ni-Cu sulfide deposit, NW China. Econ. Geol. 116, 1073–1092.
Lowenstern, J.B., 2001. Carbon dioxide in magmas and implications for hydrothermal systems. Mineral. Deposita 36, 490–502.
Mansur, E., Barnes, S.J., Ferreira Filho, C.F., 2021. The effects of post-cumulus alteration on the distribution of chalcophile elements in magmatic sulfide deposits and implications for the formation of low-S-high-PGE zones: the Luanga deposit, Carajás Mineral Province, Brazil. Can. Mineral. 59, 1453–1484.
Métrich, N., Wallace, P.J., 2008. Volatile abundances in basaltic magmas and their degassing paths tracked by melt inclusions. Rev. Mineral. Geochem. 69, 363–402.
Mungall, J.E., 2015. Physical Controls of Nucleation, Growth and Migration of Vapor Bubbles in Partially Molten Cumulates: Layered Intrusions. Springer, Netherlands, Dordrecht, pp. 331–377.
Mungall, J.E., Brenan, J.M., 2014. Partitioning of platinum-group elements and au between sulfide liquid and basalt and the origins of mantle-crust fractionation of the chalcophile elements. Geochim. Cosmochim. Acta 125, 265–289.
Mungall, J., Su, S., 2005. Interfacial tension between magmatic sulfide and silicate liquids: Constraints on kinetics of sulfide liquation and sulfide migration through silicate rocks. Earth Planet. Sci. Lett. 234, 135–149.
Mungall, J.E., Brenan, J.M., Godel, B., Barnes, S.J., Gaillard, F., 2015. Transport of metals and Sulphur in magmas by flotation of sulphide melt on vapour bubbles. Nat. Geosci. 8, 216–219.

Naldrett, A.J., Li, C., Ripley, E.M., 2011. Fundamentals of magmatic sulfide deposits, magmatic Ni-Cu and PGE deposits. Rev. Econ. Geol. 17, 1–50.
Niu, Y., 2005. Generation and evolution of basaltic magmas: some basic concepts and a new view on the origin of Mesozoic-Cenozoic basaltic volcanism in eastern China. Geol. J. China Univ. 11, 9–46.
Papike, J.J., Fowler, G.W., Adcock, C.T., Shearer, C.K., 1999. Systematics of Ni and Co in olivine from planetary melt systems: Lunar mare basalts. Am. Mineral. 84, 392–399.
Papunen, H., Mäkelä, M., 1980. Sulfur isotopes in Finnish nickel-copper occurrences. Bull. Geol. Soc. Finl. 52, 55–66.
Plank, T., Kelley, K.A., Zimmer, M.M., Hauri, E.H., Wallace, P.J., 2013. Why do mafic arc magmas contain ~4 wt.% water on average? Earth Planet. Sci. Lett. 364, 168–179.
Prichard, H.M., Knight, R.D., Fisher, P.C., McDonald, I., Zhou, M.F., Wang, C.Y., 2013. Distribution of platinum-group elements in magmatic and altered ores in the Jinchuan intrusion, China: an example of selenium remobilization by postmagmatic fluids. Mineral. Deposita 48, 767–786.
Ripley, E.M., Li, C., 2013. Sulfide saturation in mafic magmas: is external sulfur required for magmatic Ni-Cu-(PGE) ore genesis? Econ. Geol. 108, 45–58.
Ripley, E.M., Sarkar, A., Li, C., 2005. Mineralogic and stable isotope studies of hydrothermal alteration at the Jinchuan Ni-Cu Deposit, China. Econ. Geol. 100, 1349–1361.
Ripley, E.M., Taib, N.I., Li, C., Moore, C.H., 2007. Chemical and mineralogical heterogeneity in the basal zone of the Partridge River Intrusion: Implications for the origin of Cu-Ni sulfide mineralization in the Duluth complex, midcontinent rift system. Contrib. Mineral. Petrol. 154, 35.
Schoneveld, L., Barnes, S.J., Godel, B., Vaillant, M.L., Yudovskaya, M.A., Kamenetsky, V., Sluzhenikin, S.F., 2020. Oxide-sulfide-melt-bubble interactions in spinel-rich taxitic rocks of the Norilsk-Talnakh intrusions, polar Siberia. Econ. Geol. 115, 1305–1320.
Shervais, J.W., Kolesar, P., Andreasen, K., 2005. A field and chemical study of serpentinization-Stonyford, California: chemical flux and mass balance. Int. Geol. Rev. 471, 1–23.
Song, X.Y., Zhou, M.F., Wang, C., Qi, L., Zhang, C.J., 2006. Role of crustal contamination in formation of the Jinchuan intrusion and its world-class Ni-Cu-(PGE) sulfide deposit, Northwest China. Int. Geol. Rev. 48, 1113–1132.
Song, X.Y., Keays, R.R., Zhou, M.F., Qi, L., Ihlenfeld, C., Xiao, J.F., 2009. Siderophile and chalcophile elemental constraints on the origin of the Jinchuan Ni-Cu-(PGE) sulfide deposit, NW China. Geochim. Cosmochim. Acta 73, 404–424.
Song, X.Y., Danyushevsky, L.V., Keays, R.R., Chen, L.M., Wang, Y.S., Tian, Y.L., Xiao, J. F., 2012. Structural, lithological, and geochemical constraints on the dynamic magma plumbing system of the Jinchuan Ni-Cu sulfide deposit, NW China. Mineral. Deposita 47, 277–297.
Su, B.X., Robinson, P.T., Chen, C., Xiao, Y., Melcher, F., Bai, Y., Gu, X.Y., Uysal, I., Lenaz, D., 2020. The occurrence, origin, and fate of water in chromitites in ophiolites. Am. Mineral. 105, 894–903.
Su, B.X., Chen, C., Xiao, Y., Robinson, P.T., Liu, X., Wang, J., Uysal, I., Bai, Y., Sun, Y., 2021. The critical role of fluid-mediated diffusion in anomalous Fe-Mg-O isotope fractionations in ultramafic rocks of ophiolites. J. Geophys. Res. Solid Earth 126 e2020JB020632.
Tang, Z.L., Li, W.Y., 1995. Mineralisation Model and Geology of the Jinchuan Ni-cu Sulfide Deposit Bearing PGE. Geological Publishing House, Beijing.
Tang, D., Qin, K., Su, B., Mao, Y., Evans, N.J., Niu, Y., Kang, Z., 2020. Sulfur and copper isotopic signatures of chalcopyrite at Kalatongke and Baishiquan: insights into the origin of magmatic Ni-Cu sulfide deposits. Geochim. Cosmochim. Acta 275, 209–228.
Vho, A., Lanari, P., Rubatto, D., 2019. An internally-consistent database for oxygen isotope fractionation between minerals. J. Petrol. 60, 2101–2129.
Wallace, P.J., Plank, T., Edmonds, M., Hauri, E.H., 2015. Volatiles in magmas. In: The Encyclopedia of Volcanoes. Elsevier, pp. 163–183.
Wei, B., Wang, C.Y., Lahaye, Y., Xie, L., Cao, Y., 2019. S and C isotope constraints for mantle-derived sulfur source and organic carbon-induced sulfide saturation of magmatic Ni-Cu sulfide deposits in the Central Asian Orogenic Belt, North China. Econ. Geol. 114, 787–806.
Yang, X.Z., Ishihara, S., Zhao, D.H., 2006. Genesis of the Jinchuan PGE deposit, China: evidence from fluid inclusions, mineralogy and geochemistry of precious elements. Mineral. Petrol. 86, 109–128.
Yang, S.H., Yang, G., Qu, W.J., Du, A.D., Hanski, E., Lahaye, Y., Chen, J.F., 2018. Pt-Os isotopic constraints on the age of hydrothermal overprinting on the Jinchuan Ni-Cu-PGE deposit, China. Mineral. Deposita 53, 757–774.
Yao, Z.S., Mungall, J.E., 2020. Flotation mechanism of sulphide melt on vapour bubbles in partially molten magmatic systems. Earth Planet. Sci. Lett. 542, 116298.
Yao, Z.S., Mungall, J.E., Qin, K.Z., 2019. A preliminary model for the migration of sulfide droplets in a magmatic conduit and the significance of volatiles. J. Petrol. 60, 2281–2316.
Zhang, M.J., Kamo, S.L., Li, C., Hu, P.Q., Ripley, E.M., 2010. Precise U-Pb zircon-baddeleyite age of the Jinchuan sulfide ore-bearing ultramafic intrusion, western China. Mineral. Deposita 45, 3–9.